

## IMAGING THE FOREARC IN SOUTH CENTRAL CHILE

Susan Beck<sup>1</sup>, Mallory Morell<sup>1</sup>, Kevin Ward<sup>1</sup>, Berk Biryol<sup>1</sup>, George Zandt<sup>1</sup>,  
Steve Roecker<sup>2</sup>, Anne Meltzer<sup>3</sup>, Lucy Brown<sup>3</sup>, Ray Russo<sup>4</sup>, Harley Benz<sup>5</sup>

<sup>1</sup>Department of Geosciences, University of Arizona, Tucson, Arizona, USA

<sup>2</sup>Department of Earth and Environmental Sciences, Rensselaer Polytechnic Institute, Troy,  
New York, USA

<sup>3</sup>Department of Earth and Environmental Sciences, Lehigh University, Bethlehem,  
Pennsylvania, USA

<sup>4</sup>Department of Geological Sciences, University of Florida, Gainesville, Florida, USA

<sup>5</sup>National Earthquake Information Center, U.S. Geological Survey, Golden Colorado, USA

### INTRODUCTION

The  $M_w=8.8$ , Maule earthquake that occurred off the coast of Chile on February 27, 2010 is one of the largest megathrust earthquakes ever to be recorded and ruptured ~600 km of the plate boundary. This segment of the Nazca-South America plate boundary is an ideal region to investigate the processes related to the structure of the down-dip edge of the seismogenic zone, forearc, and subducting slab. Immediately after the Maule earthquake, international teams from France, Germany, Great Britain, and the United States joined Chilean seismologists to install seismic stations between 33°-38.5°S, from the coast to the foothills of the Andes to produce the International Maule Aftershock Deployment (IMAD) data set (Figure 1A). These stations were deployed starting in mid-March with some stations pulled out in late September while others remained recording until the end of December of 2010. We have used broadband seismic data from the IMAD stations as well as other temporary and permanent broadband stations in the south central Andes to locate and determine focal mechanisms of aftershocks, and image the forearc and the down going slab (Figure 1).

### AFTERSHOCK LOCATIONS AND FOCAL MECHANISMS

In order to integrate these data into a unified catalog, the USGS National Earthquake Information Center develop procedures to use their real-time seismic monitoring system (Bulletin Hydra) to detect, associate, location and compute earthquake source parameters from these stations. As a first step in the process, the we built a reviewed catalog of approximately 2100 M 4.0 or larger earthquakes for the time period of the main aftershock deployment from March 2010-December 2010 (Figure 1B). The catalog includes earthquake locations, magnitudes ( $M_l$ ,  $M_b$ ,  $M_b\_BB$ ,  $M_s$ ,  $M_s\_BB$ ,  $M_s\_VX$ ,  $M_c$ ), associated phase readings and regional moment tensors solutions. Tuning of automated detection and association parameters generated catalog of some 44,000 events to approximately M2.0. We characterize the aftershock sequence in terms of magnitude, frequency, and location over time. Using the catalog locations and travel times as a starting point we use double difference techniques to investigate relative locations and earthquake clustering. In addition, phase data from candidate ground truth events and modeling of surface waves can be used to calibrate the velocity structure of central Chile to improve the real-time monitoring.

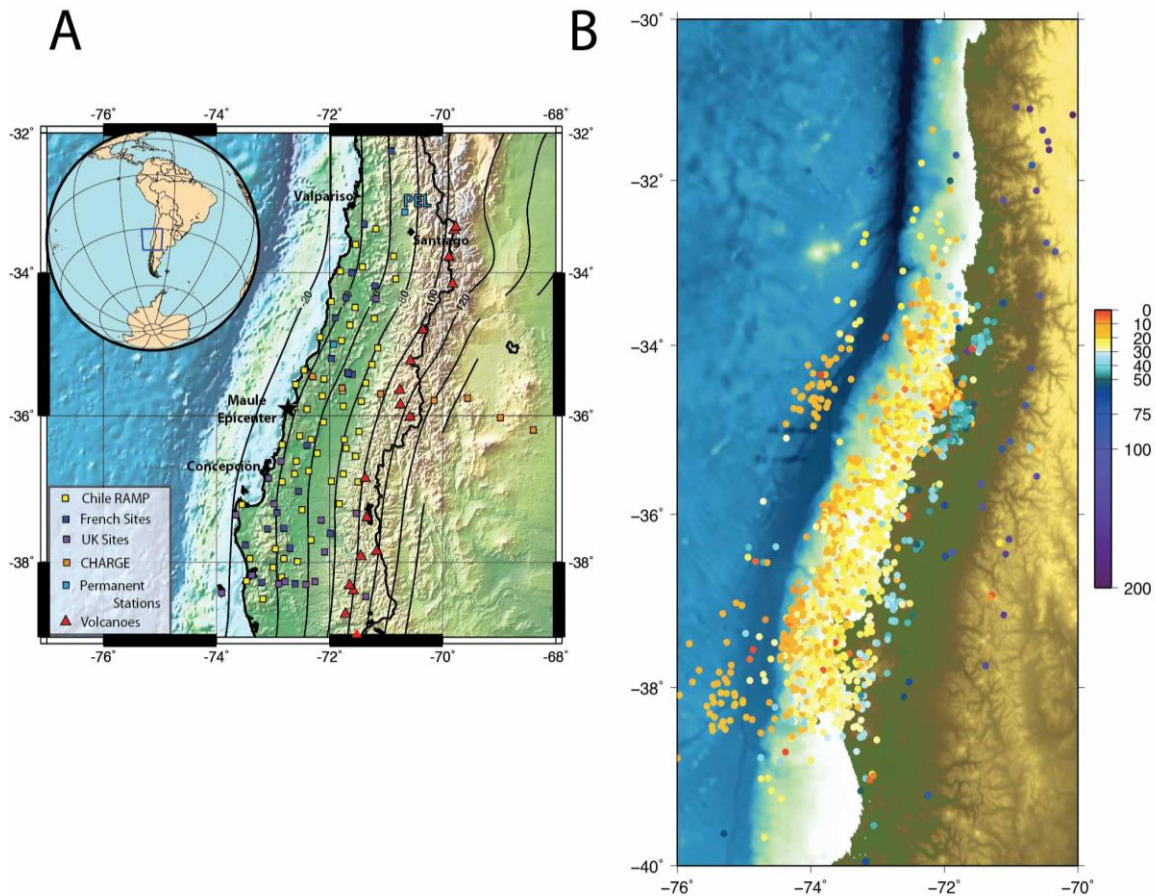


Figure 1. (a) Map of the IMAD and other temporary and permanent seismic stations along in Chile and western Argentina. Holocene volcanoes are shown in red triangles. (b) Map of relocated Maule Earthquake aftershocks with  $M \geq 4.0$  in this study. Colors represent the depth of the event.

## SEISMIC IMAGING WITH RECEIVER FUNCTIONS AND AMBIENT NOISE TOMOGRAPHY

We calculated receiver functions (RFs) from teleseismic P and PP phases and constructed common conversion point stacks to image the structure of the slab and forearc region down to a depth of  $\sim 120$  km. We have migrated the RF with a simple 1-D velocity model ( $V_p=6.5$  km/s and  $V_p/V_s=1.8$  above 35 km and  $V_p=8.0$  km/s and  $V_p/V_s=1.8$  below 35 km) following the method of Gilbert et al (2004) (Figure 2). We have identified the oceanic slab Moho on several E-W and N-S profiles at 40 to 60 km depth beneath the array and several discontinuities above the slab in the forearc (Figure 2). We also image a prominent Ps conversion that we interpret as the continental Moho at  $\sim 35$  km under the foothills of the Andes and decreasing to 25-30 km under the central valley of Chile. This prominent Ps conversion we interpret as the Moho ends at  $\sim 72^\circ$ W longitude on the E-W cross-section (Figure 2). We observe a prominent Ps conversion at  $\sim 40$ -50 km depth on a NNE-SSW cross-section parallel to the strike of the slab that we interpret as the oceanic Moho in the down-going slab. There is an intermittent decrease in velocity above the red that may be the top of the oceanic crust and or sediments being subducted.

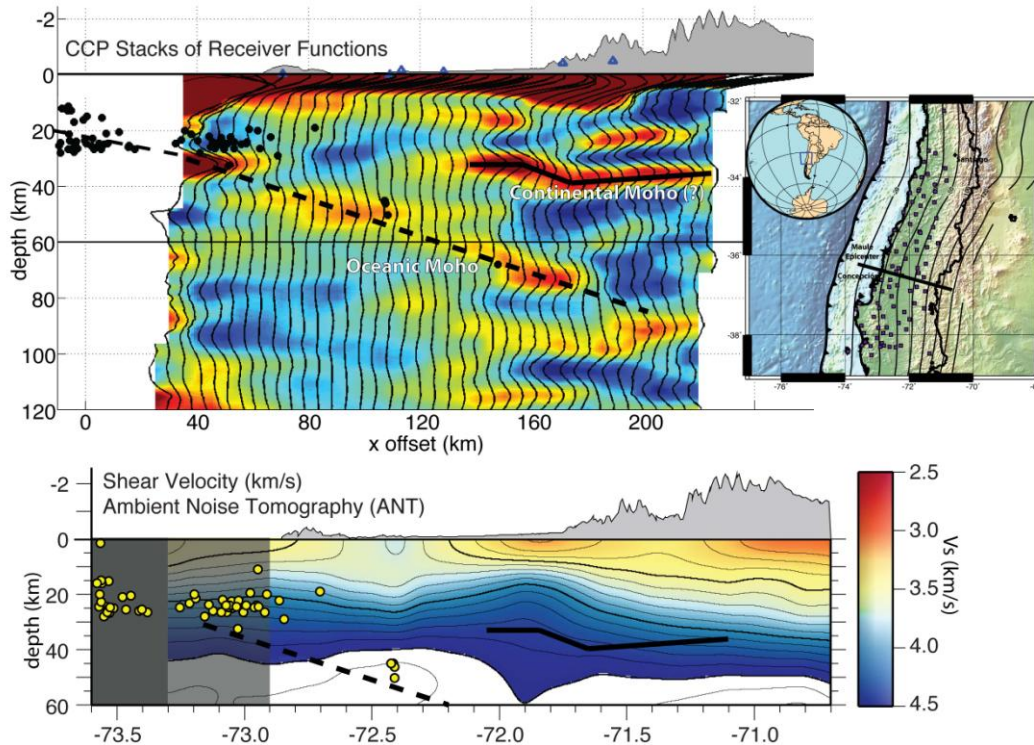


Figure 2. Cross-section of receiver function CCP stacks with 5 km bin spacing in the EW direction and 15 km in the NS direction migrated with a simple 1-D velocity model (above). Cross-section of ambient noise tomography showing absolute shear wave velocity across the Chile forearc (below). The earthquakes plotted are relocated aftershocks compressed ~10 km on either size of the cross section line. Map shows the location of the both cross-sections.

We have used IMAD stations and other temporary and permanent broadband seismic stations in Chile and Argentina for Ambient Noise Tomography (ANT) to obtain absolute shear velocities in the crust. We have used ambient noise between periods of 8 and 40 sec to construct phase velocity maps following the method of Bensen et al., (2007). We then invert the phase velocities for a 3-D shear-wave velocity at  $0.1^\circ$  grid spacing using a constant velocity starting model. Figure 3 shows a map view of the resultant shear velocities at depths of 8 and 25 km. At shallow depths the basins in the backarc of the Sierras Pampeanas in Argentina show clear low shear wave velocities. The Chile forearc has higher shear velocities ( $>3.8$  km/s) at all depths between  $32^\circ$  and  $38^\circ$ S. Much of the active arc shows lower shear wave velocities ( $<3.5$  km/s) at mid and lower crustal depths consistent with warm temperatures. The region above the flat slab, near  $\sim 31^\circ$ S, where the arc shut off at 6-8 Ma, shows only slightly higher shear wave velocities at  $\sim 25$  km depth as compared to the active arc to the south.

## SUMMARY

We are constructing a unified catalog of 2010 Maule earthquake aftershocks to better image the seismogenic zone. The receiver functions and ambient noise tomography are the first step toward imagining the Chile forearc and arc. We are using teleseismic and local relocated

earthquakes for travel time tomography to determine a P-wave velocity model for the forearc and arc. Future work will include relocating additional aftershocks, particularly the events near the down-dip edge of the Maule mainshock rupture zone and comparing the locations to the seismic imagines of the Chile forearc.

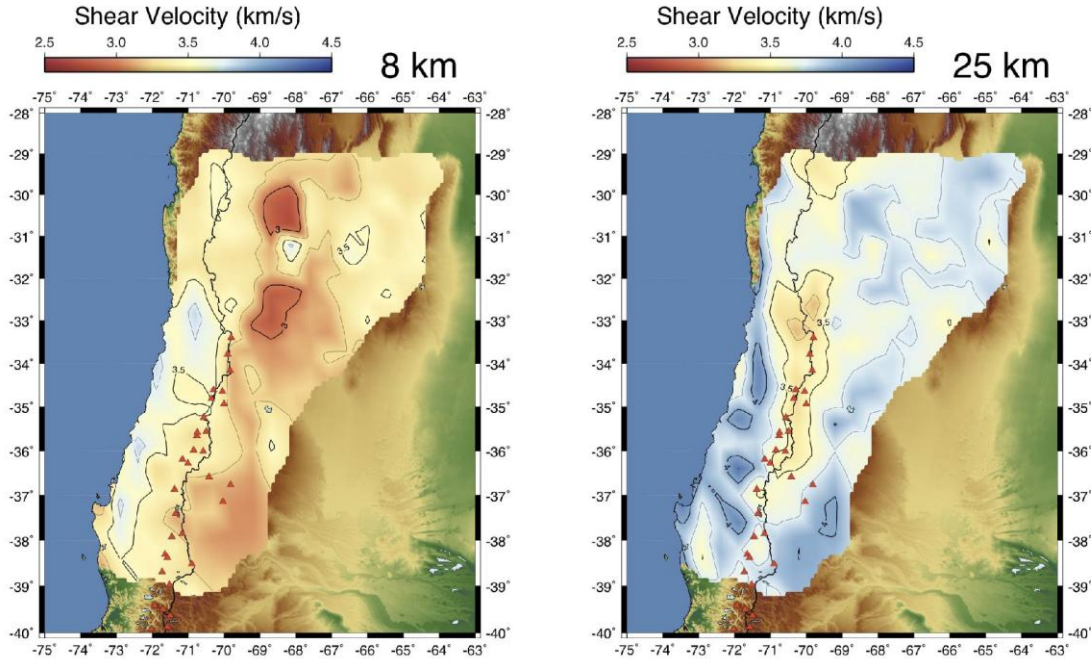


Figure 3. Map view of shear wave velocities from ambient noise tomography at depth slices of 8 and 25 km. Active volcanoes are shown as red triangles.

## ACKNOWLEDGMENTS

We thank all the participants of the IMAD deployment teams for making their data open. We especially thank Sergio Barrientos, Klaus Bataille, Diana Comte, Andreas Rietbrock, Fredrick Tilmann, Ben Heit, Dietrich Lange, Pascal Bernard, Jean-Pierra Vilotte and the entire IRIS CHAMP team. This work was supported by NSF award numbers 1045597, 1036352, and 1036349.

## REFERENCES

- Bensen, G. D., M. H. Ritzwoller, M. P. Barmin, A. L. Levshin, F. Lin, M. P. Moschetti, N. M. Shapiro, and Y. Yang, 2007, Processing seismic ambient noise data to obtain reliable broad band surface wave dispersion measurements, *Geophys. J. Inter.*, **169**(3), 1239-1260, doi: 10.1111/j.1365-246X.2007.03374.x.
- Gilbert, H.J. and A.F. Sheehan, 2004, Images of crustal variations in the intermountain west, *J. Geophys. Res.*, **109**, B03306, doi:10.1029/2003JB002730.